Aerospace Science and Technology 98 (2020) 105654

Contents lists available at ScienceDirect

Aerospace Science and Technology

www.elsevier.com/locate/aescte

Transient analysis of upstream wake inside turbine blade passage with purge flow

Babu Sushanlal, S. Anish *

Turbomachinery Laboratory, Mechanical Department, National Institute of Technology, Karnataka, India

ARTICLE INFO

Article history:
Received 19 June 2019
Received in revised form 28 October 2019
Accepted 17 December 2019
Available online 20 December 2019

Keywords:
Secondary vortex
Purge flow
Q-criterion
Karman vortex
Exit yaw angle
Vortex filament

ABSTRACT

Secondary air bled from the compressor which bypasses the combustion chamber is used to seal the turbine components from incoming hot gas. Interaction of this secondary air (also known as purge flow) with the mainstream flow can alter the flow characteristics of turbine blade passage. This paper presents numerical investigation of interaction between ejected purge flow and mainstream flow in the presence of upstream disturbances/wakes. Steady as well as unsteady simulations are carried out using Reynolds Averaged Navier Stokes equations and SST turbulence model. The numerical results are validated with experimental measurements obtained at the blade exit region using an L shaped 5 hole probe and Scanivalve. Upstream wakes are generated by a circular cylinder, kept upstream of blade leading edge at different pitch-wise positions. For transient analysis cylinders are kept at stagnation line (STW) and middle of the blade passage (MW). The analysis reveals the interaction effects of two more additional vortices, viz. the cylinder vortex (Vc) and the purge vortex (Vp). Steady state analysis shows an increase in the underturning at blade exit due to the squeezing of the pressure side leg (PSL) of horse shoe vortex towards the pressure surface by the cylinder vortices (Vp). The unsteady analysis reveals the formation of filament shaped wake structures which breaks into smaller vortical structures at the blade leading edge for STW configuration. These filaments lead to the formation of additional pressure surface vortices. On the contrary, in MW configuration, the obstruction created by the purge flow causes the upper portion of cylinder vortices bend forward, creating a shearing action along the spanwise direction. In MW configuration, the horse shoe vortices generated from the upstream cylinder are broken by the purge vortex whereas in the STW configuration it slides over the purge vortex and move towards the suction surface under the influence of the pitchwise pressure gradient.

1. Introduction

One of the primary objective of the modern gas turbine engine designers is to reduce secondary losses which are responsible for the total pressure losses especially within the high pressure, low aspect ratio turbine blade passages. Novel passive techniques such as leading edge fillet [1–3], endwall fence [4], dynamic hump [5], endwall contouring [6,7] and recent bio-inspired biomimetic trailing edge [8] has been reported for secondary loss reduction in recent years. The passive techniques gain more attraction than active technique because of the absence of additional energy expenditure.

In gas turbines there exists an unavoidable gap between the rotor and stator disk, usually known as seal gap or wheel space, through which the hot ingress will take place. To minimize the ingress a sealant flow bled from the compressor is fed through the seal gap which purges and reduces hot ingress and provides cooling. Numerous works related to upstream slot cavity flow and discrete hole film cooling are available in recent years. Friedrichs et al. [9,10] used ammonia and diazo coating technique to determine the endwall film cooling effectiveness (FCE). To provide more endwall protection new film hole arrangements were proposed and the film hole locations were rearranged by keeping coolant flow rate constant [11]. Barigozzi et al. [12] observed that fan shaped film holes on flat endwall provided better endwall cooling than cylindrical holes at low coolant ejection rates. Many other design variations had been reported to improve the FCE without generating much thermodynamic penalties. The use of fins in the purge slot, contoured endwall with trenched holes, pressure side cut back trailing edge, optimizing the purge slot width, purge hole diameter and purge ejection angle are few of such parameters [13–19].

* Corresponding author.
E-mail addresses: sushanlalbabume@gmail.com (B. Sushanlal), anish@nitk.edu.in (S. Anish).

https://doi.org/10.1016/j.ast.2019.105654
1270-9638/

Nomenclature

B	Blade pitch	(mm)
C_{ax}	Axial chord length	(mm)
C_b	Blade loading coefficient	
C_p	Static pressure coefficient	
C_{po}	Local total pressure loss coefficient	
$\overline{C_{po}}$	Pitch averaged total pressure loss coefficient	
$\overline{\overline{C_{po}}}$	Mass averaged total pressure loss coefficient	
H	Total span	(mm)
HSV	Horse-shoe vortex	
LE	Leading edge	
m_c	mass flow rate at coolant inlet	(kg/s)
m_∞	mass flow rate at mainstream inlet	(kg/s)
M	Velocity ratio	
PS	Pressure surface	
PScv	Pressure side corner vortex	
PSL	Pressure side leg of HSV	
PSv	Pressure surface vortex	
PV	Passage vortex	
P_s	Static pressure	(Pa)
P_t	Total pressure	(Pa)
$P_{t,c}$	Total pressure at coolant inlet	(Pa)
$P_{t,\infty}$	Total pressure at mainstream inlet	(Pa)
Re	Reynolds number	
SS	Suction surface	
SSL	Suction side leg of HSV	
TE	Trailing edge	
TKE	Turbulent kinetic energy	
U_c	Coolant average inlet velocity	(m/s)
U_∞	Mainstream average inlet velocity	(m/s)
Vc	Cylinder vortex	
Vp	Purge vortex	
μ	Dynamic viscosity	(Pa S)
ρ_c	Coolant density	(kg/m^3)
ρ_∞	Mainstream air density	(kg/m^3)
τ	Non-dimensionalized time	

Flow field measurements obtained by Burd et al. [20] on engine representative nozzle guide vane with contoured and flat endwall suggested streamwise momentum of the ejected coolant had thinned the inlet boundary layer and reduced the passage cross flow. Oke et al. [21] showed rather than double slot injection, single slot injection provides more uniform coolant distribution at the blade leading edge while inside the passage both cases were similar. Kost and Nicklas [22] described the outcomes of strong coolant-mainstream interaction inside the blade passage and stated that detrimental effects of coolant ejection increases flow turbulence which was later confirmed by Liu and Yang [23]. Nicklas [24] identified an increase in Mach number at downstream trailing edge region where cooling becomes extremely difficult and suggested additional trailing edge cooling methods to provide better platform protection. Angular orientation of film holes towards pressure surface significantly reduces cross flow and provides better protection along pressure side-endwall corner [25].

An important parameter in the purge flow cooling is the blowing ratio. It is also defined as coolant to mainstream mass flux ratio. Liu et al. [26] proposed that inline arranged double row staggered film holes can provide more uniform cooling to the blade platform at higher blowing ratios. Oil dot visualization and mass transfer analysis conducted by Papa et al. [27] revealed that at lower blowing ratios coolant entrained into the passage vortex, climbs up the blade suction surface, hardly cooling the blade endwall and pressure side. Cascade analysis carried out by Chen [28] and Chowdhury et al. [29] explored the effects of inlet purge swirl, blowing ratio, density ratio and coolant to mainstream mass flow ratio (MFR) values over endwall cooling. Introduction of upstream swirl purge flow and slash-face leakage flow along with different film hole configurations gives more desirable platform coolant distribution and development of secondary vortices inside the blade passage. Cui and Tucker [30] numerically investigated the effects of upstream disturbances and secondary flows over the downstream blade passage in the presence of purge flow and the authors identified additional loss generation regions at the interface of suction surface and endwall.

The purge flow cooling becomes more challenging with the presence of an upstream disturbance/wake. Few researchers have studied this effect by simulating the wakes by stationary or rotating cylinders [31–35]. Yefi et al. [36] simulated non-uniform inlet temperature profile and swirl distribution in between the combustor and high pressure vanes and stated that non-uniformity in the heat load influences axial temperature distribution between the successive blades while swirl orientation dominates radial temperature distribution. Kai Zhon et al. [37] found that, periodic interaction of unsteady upstream passage vortex has reduced the minimum axial length of tip leakage vortex breakdown by 15% which improved the overall aerodynamic performance. Zerobin et al. [38] analyzed the generation of unsteady pressure patterns by the stator-rotor interaction on a one and half stage experimental test facility consisting of HPT, turbine center frame (TCF) and LPT vane. In another comprehensive study he analyzed the effects of individual tip and hub purge flow on TCF aerodynamics and concluded that, total pressure loss of TCF can be effectively lowered by proper reduction of purge flow rate [39,40]. Influence of different wake profiles on boundary layer transition and suction side separation are numerically explained by Hammer et al. [41]. He observed that, weaker wakes lead to the generation of large and long lasting separation bubbles and increased profile losses. Choi et investigated the effects of wake on flow and thermal endwall characteristics at different Strouhal numbers. The disturbed secondary vortices induced by the wake made the heat transfer distribution over the endwall more uniform compared to non-wake case [42]. A good improvement in the net heat flux reduction rate was observed with aero and heat transfer optimized endwall and mate face gap leakage flow [43–45].

Most of the literatures on purge flows have focused on blade endwall thermal protection and overall flow modification specifically at blade exit regions. Some features such as evolution of vane trailing edge wakes (upstream disturbance) and its interaction with purge and mainstream flow are neglected and needs more attention. The dependency of wake structure or its geometrical appearance on time as well as space needs to be quantified. The objective of this paper is to understand the formation of additional secondary vortices generated by the interaction of upstream wakes and purge flow within the turbine blade passage. The formation and transient propagation of the vortical structures are analyzed. The upstream disturbances are generated by a stationary cylindrical rod which is kept at 35% axial chord (C_{ax}) distance upstream of the blade leading edge. Such an analysis is helpful in understanding their influence on the flow characteristics such as, suction side flow separation, pressure surface vortex formation, blade exit yaw angle and blade exit total pressure loss coefficient. To improve the quality of numerical analysis, simulations are carried out using Unsteady Reynolds Averaged Navier Stokes (URANS) equation

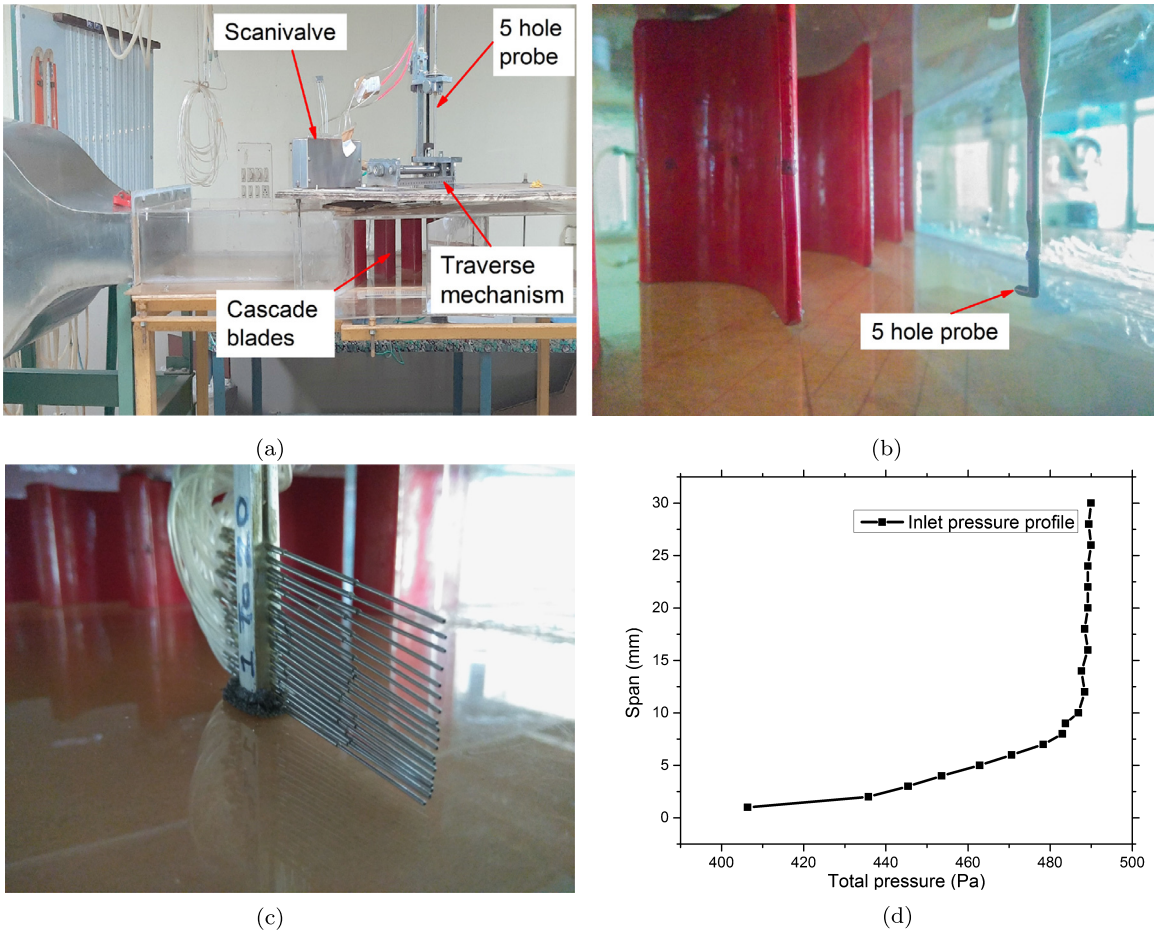

Fig. 1. a) Wind tunnel with linear cascade test section b) 5 hole probe installed at cascade exit c) Boundary layer rake installed at cascade inlet d) Total pressure profile at inlet.

by varying the relative position of the upstream cylinder in pitch-wise direction.

2. Methodology

Primarily, numerical investigations are carried out to achieve the above stated objectives. Few experiments have also been carried out to validate the numerical results. This section details the methodologies adopted for both experimental as well as numerical studies.

The linear turbine cascade chosen for the present analysis is a high pressure low aspect ratio turbine blade available at the Turbomachinery Laboratory of National Institute of Technology, Karnataka. Turbine blade parameters and specifications are described in Table 1 and the test facility is shown in Fig. 1a. The experimental facility consists of a five hole pressure probe (tip diameter of 2.05 mm) (Fig. 1b) with a traverse mechanism at the downstream of the blades. The pre-calibrated probe has been moved in the span-wise and pitch-wise directions in steps of 1 mm near to endwall and 5 mm away from endwall. The stem of the pressure probe has been kept along the spanwise direction and probe tip was aligned with the blade exit design angle. The traverse mechanism can cover 1.8 times cascade pitch over a full span range. All pressures were measured using 16-port Scanivalve system and signals were sampled for 0.1 sec at a frequency of 2000 Hz. The obtained readings are used to derive the flow parameters including flow angle and the total pressure. At the upstream side of the blades, a boundary layer rake (Fig. 1c) is used to measure the incoming total pressure profile and the resulting profile is shown

Table 1
TURBINE BLADE PARAMETERS.

Inlet flow angle	45^0(from axial direction)
Blade exit angle	-66.3^0(from axial direction)
Total blade turning angle	118.3^0
Blade axial chord length	100 mm
Blade pitch	112 mm
Blade span	120 mm
Re	2 X 10^5
Zweifel loading coefficient	1.18

in Fig. 1d. A series of holes of diameter 0.7 mm, have been drilled perpendicular to the blade surface at the midspan location to measure the static pressure. The measurement using five hole probe and surface pressure holes have an uncertainty of +/-1% and the measured yaw angle has an uncertainty of $+/-0.5^0$.

For numerical analysis a single blade passage with periodic boundary conditions at side walls are selected. The domain inlet is kept at 1.5 times the axial chord distance upstream of the blade leading edge and the outlet plane at two times the axial chord distance downstream from the trailing edge. The purge slot has a width of 7 mm, length of 50 mm and inclination angle 45^0, is located at 11% C_{ax} upstream of the blade leading edge [13]. Purge flow is ejecting at a velocity ratio (M) of 0.6, where velocity ratio is defined as the ratio of coolant inlet average velocity to the mainstream inlet average velocity. Cylinders of diameter 6 mm, which represent the blade trailing edge [42,46], are kept at 35% C_{ax} upstream of blade leading edge (LE) at four different locations obtained by dividing the blade passage into quarters [46]. Posi-

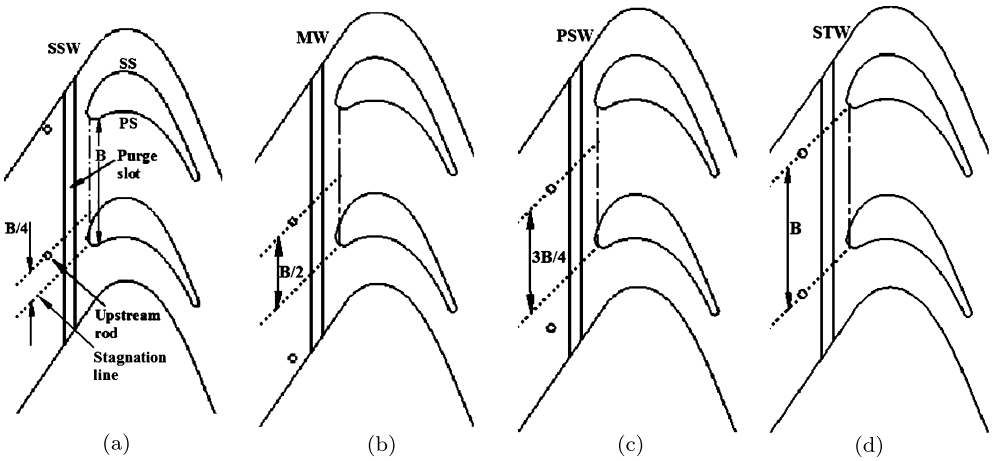

Fig. 2. Computational domain with cylindrical rods at different locations.

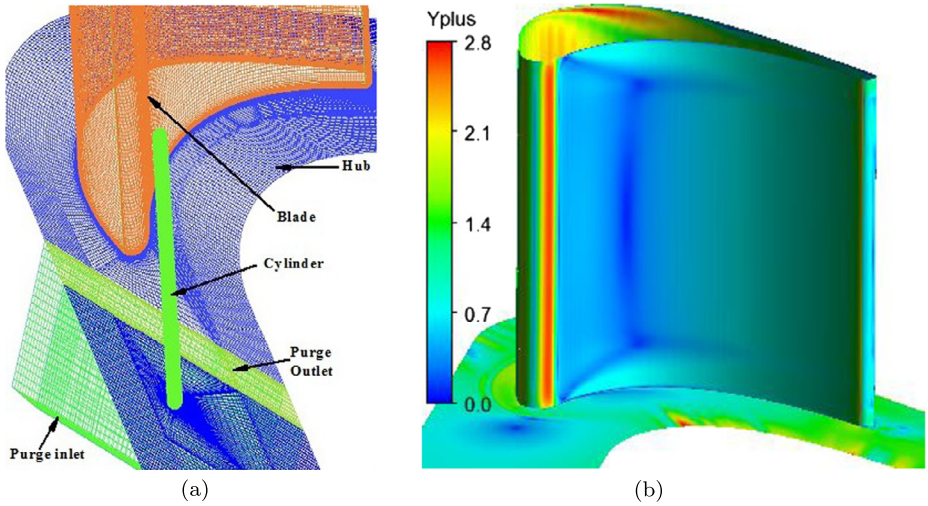

Fig. 3. Structured mesh and Y+ distribution over the blade and hub endwall.

tion of the cylinders with respect to stagnation line of mainstream flow are shown in Fig. 2 and these configurations are named as Suction side wake (SSW), Mid passage wake (MW), Pressure side wake (PSW) and Stagnation wake (STW).

Both Steady and Unsteady Reynolds Averaged Navier Stokes equations are solved by using ANSYS-CFX. ANSYS CFX uses a coupled solver, which solves the Navier Stokes equations (for velocity and pressure) as an implicitly coupled single system. The turbulence is modeled with two-equation shear stress transport (SST) model. The capability of SST turbulence model for simulations related to turbine cascade, has already been established in several literatures [42,47–50].

Commercial mesh generation program ICEM-CFD is used to create fully structured grid for the entire computational domain (Fig. 3a). At boundary layer regions, mesh refinement is achieved by providing O-type grid around blade & upstream cylinder surfaces and hexahedral mesh for rest of the domain. Maximum y+ value obtained for the fully structured mesh is 2.8 (Fig. 3b). Air as ideal gas which represents compressible viscous flow, is used as the working fluid. At the inlet, total pressure profile obtained from the experiment and 5% turbulence intensity obtained with the help of DANTEC 1D wire probe hot wire anemometer are specified while at the outlet mass flow rate is mentioned. Inlet velocity of 10.73 m/s is specified at purge inlet. Accordingly the mass averaged total pressure and volume flow rate calculated at purge inlet are 391.85 Pa and 0.008416 m^3/s respectively. At one pitch distance translational periodic boundary condition is used. The mainstream flow is blown at room temperature whereas the secondary air enters at higher temperature (55^0C), resulting in a density ratio of about 0.92 [13,17,51].

For transient analysis, advection terms of momentum equations are evaluated using second-order accurate and bounded high-resolution scheme whereas for diffusion terms, shape functions are used to evaluate spatial derivatives. High resolution scheme uses a second order scheme as far as possible and blends to a first order scheme to maintain boundedness. It contains far less numerical diffusion. Also time discretization is achieved by Second Order Backward Euler scheme. Since the cylinder is kept stationary, time required for fluid to travel the full blade passage from leading edge to trailing edge is chosen as one period (one cycle). This time period is resolved with 55 time steps (τ) and each time step (τ) duration is 0.0001 seconds [52]. The simulations are carried out for several cycles (16 time periods) and the results are taken from the last cycle. A series of inner loop iterations were carried out after each time step until convergence is achieved in order to correct the non-linearities for the output of that given time. During the simulations, variation of velocity at six locations (three before leading edge and three after trailing edge) are monitored with respect to time to ensure the numerical stability.

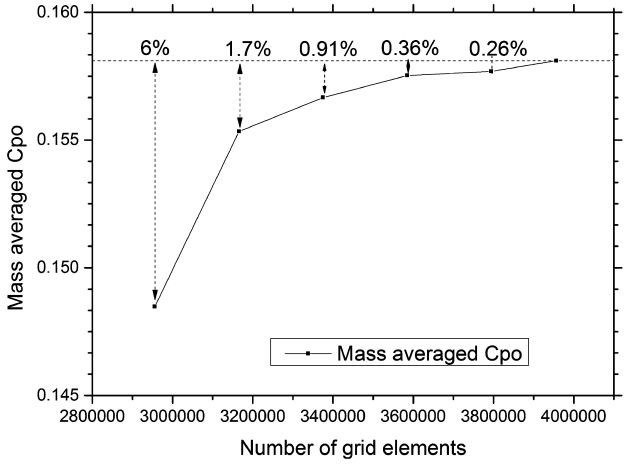

Fig. 4. Grid Independence study.

3. Verification and validation

Grid sensitive study has been carried out for all the configurations to identify the optimum number of grid elements. Fig. 4 depicts the grid sensitivity analysis for base case (without purge and without upstream wake). Different mesh sizes selected for baseline case are 2.95 million, 3.16 million, 3.37 million, 3.58 million, 3.79 million and 3.95 million. No significant difference has been observed in the results with 3.58 million, 3.79 million and 3.95 million. Based on the results obtained, 3.58 million mesh elements are chosen for the base case domain. At 3.58 million mesh elements, variation in the mass averaged total pressure loss coefficient is 0.36% in comparison with the finest mesh (3.95 million). Similarly optimum mesh size selected for purge and purge with cylinder cases are 3.74 million and 4.13 million respectively. The number of mesh elements versus mass averaged total pressure loss coefficient at 135% C_{ax} is shown in Fig. 4.

The validation of numerical results has been carried out for the base case (BC) and base case with cylinder in stagnation line (BC-STW). The parameters considered for the validation are static pressure coefficient (C_p) distribution around the blade surface at different inlet velocities (14.42 m/s, 19.23 m/s, 24.04 m/s), pitch averaged exit yaw angle deviation at 127% C_{ax} (for BC & BC-STW) and local total pressure loss coefficient (C_{po}) distribution at 127% C_{ax} (for BC & BC-STW). The Static pressure coefficient (C_p) is obtained from the static pressure ports provided at blade midspan and pitch averaged yaw angle deviation and total pressure loss coefficient are obtained from measurements through the five hole probe at cascade exit. The static pressure and total pressure loss values are normalized with respect to inlet dynamic pressure to obtain the C_p (Eq. (1)) and C_{po} (Eq. (2)) respectively. Fig. 5a shows that static pressure coefficient predicted through numerical simulations are quantitatively and qualitatively matching well with the experimental results. Similarly the exit yaw angle deviation (Fig. 5b) and the total pressure loss coefficient (Fig. 6) are also compared with the experimental results.

$$C_p = \frac{P_s}{0.5\rho_\infty U_\infty^2} \tag{1}$$

$$C_{po} = \frac{\frac{m_\infty}{m_\infty+m_c}\overline{\overline{P_{t,\infty}}} + \frac{m_c}{m_\infty+m_c}\overline{\overline{P_{t,c}}} - P_t}{0.5\rho_\infty U_\infty^2} \tag{2}$$

It is well understood that the total pressure loss coefficient values are the most crucial and difficult parameter to get a closer match with RANS simulations. Hence the local values of loss coefficient at 127% C_{ax} is plotted in the form of a contour and compared with the experimental results. A better match is observed at majority of the regions including near the endwall. At loss core regions, numerical simulation is found to be slightly over-predicting (maximum deviation of 14.2% is noticed). However, a RANS simulation predicts the mean flow behavior with reasonable accuracy [50, 53–55] and it is very useful in predicting the overall performance analysis of the turbine blade.

4. Results and discussion

The flow modifications caused by the interaction of upstream wake with the purge flow are analyzed in this section. These interactions lead to the formation of additional vortices in the blade passage. These additional vortices are identified and their influence on the blade loading, exit yaw angle and turbulence kinetic energy are discussed in the initial part of this section. At the latter part, detailed unsteady analysis are carried out to understand the transient behavior of these vortices and their influence on the loss coefficients.

4.1. Effect of upstream wake on general flow behavior

In order to understand the flow modifications caused by the interaction of upstream wake and purge flow, iso-surface Q-criterion superimposed with streamwise vorticity distribution inside the

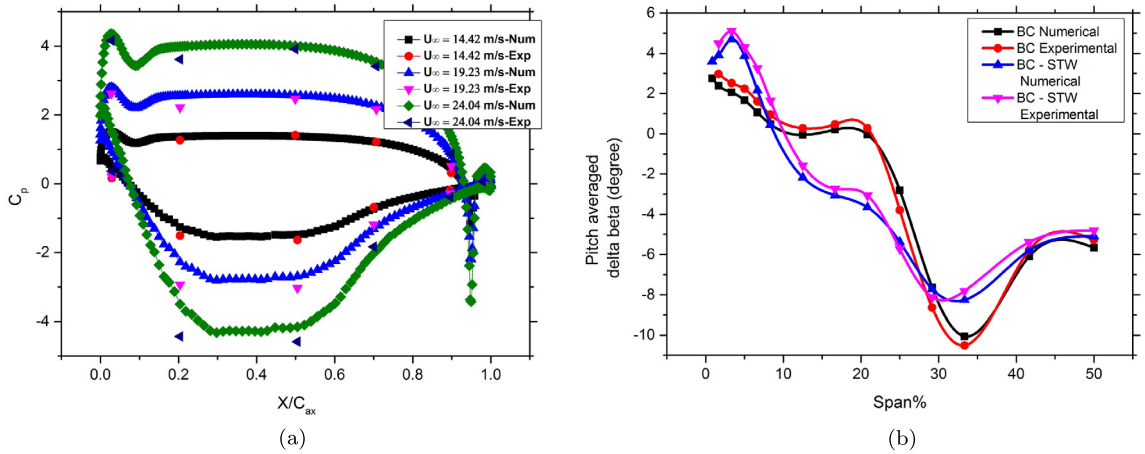

Fig. 5. Validation of numerical results using Static pressure coefficient distribution at blade midspan (BC) and pitch averaged exit yaw angle deviation at 127% C_{ax} (BC and BC-STW).

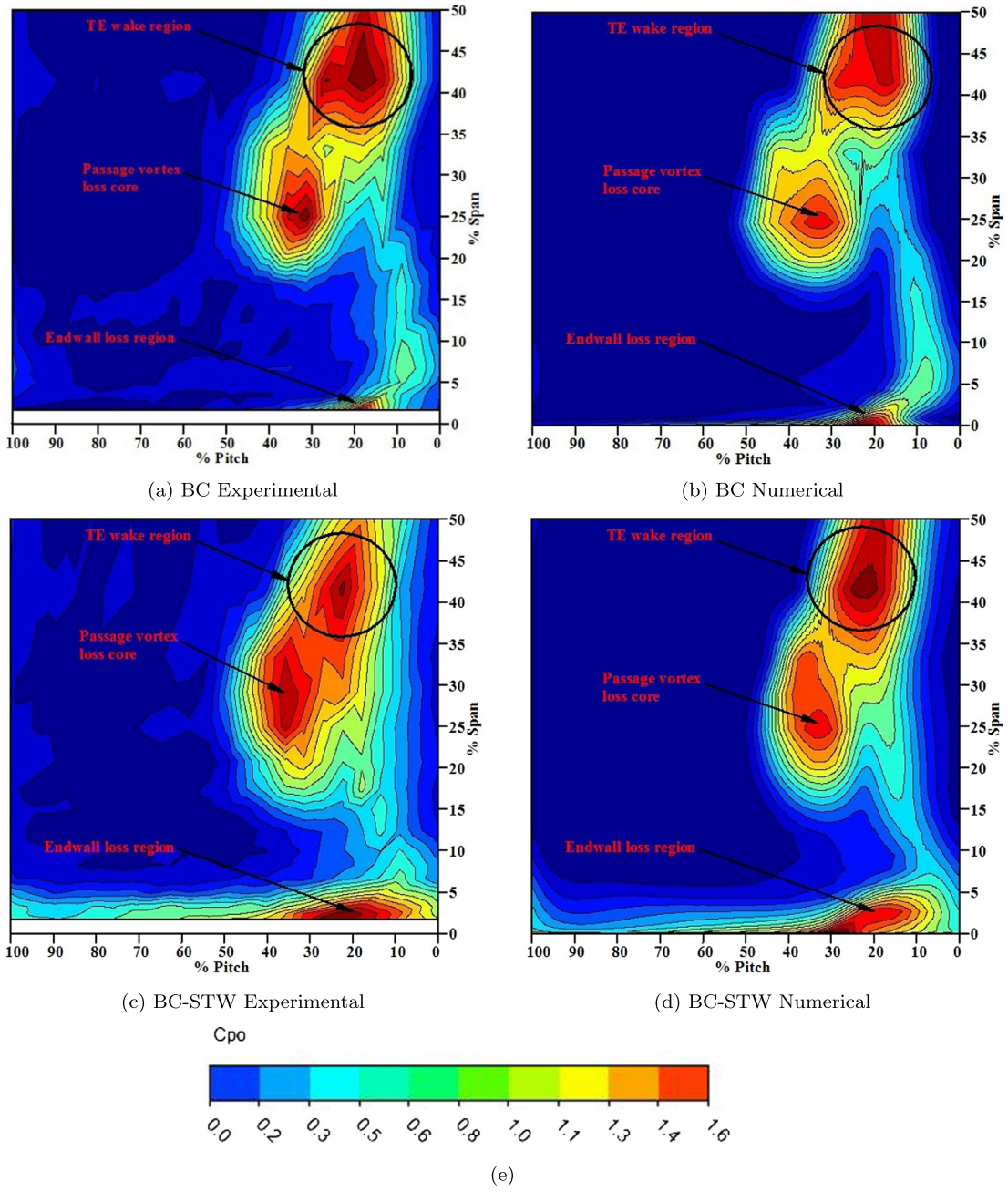

Fig. 6. Validation of numerical results using local total pressure loss coefficient at 127% C_{ax}.

blade passage is analyzed (Fig. 7). Rotational direction of suction side leg (SSL) and pressure side leg (PSL) of horse shoe vortex can be identified as clockwise (positive sense of rotation) and counter clockwise (negative sense of rotation) respectively. Apart from the horse shoe vortex and passage vortex, four more additional vortices can be identified. They are pressure surface vortex (PSv), pressure side corner vortex (PScv), purge vortex (Vp) and cylinder vortex (Vc). It is observed that for all the cases the purge vortex (Vp) is dragged towards the suction surface due to the transverse pressure gradient. In SSW configuration, Vc merges with SSL just downstream of leading edge and later both combines with the PSL at the aft part of suction surface (Fig. 7c). As the cylinder position shifts towards the pressure side the strength of Vc increases. When the cylinder is near the stagnation region of the blade (Fig. 7f), the cylinder vortex (Vc) pushes the PSL towards the pressure surface making the flow more attached to the pressure surface near to endwall. The formation of pressure surface vortex (PSv) may be attributed to the increased span-wise pressure gradient caused by the purge flow. The span-wise pressure gradient causes the rolling up of low momentum fluid inside the pressure side bubble (PSB) to generate the PSv. In STW configuration, cylinder wakes (Vc) suppresses the pressure side bubble formation which results in the reduction of spanwise pressure gradient over the pressure surface and leads to the upward movement of PSv (Fig. 7f).

4.2. Effect on the blade loading

In order to understand the effect of upstream wake and purge flow on blade loading the static pressure coefficient (C_p) has been plotted at 4.1% and 50% span. The results have been presented along normalized axial chord (X/C_{ax}) for all the configurations. At midspan strong acceleration on the suction side of the blade is re-

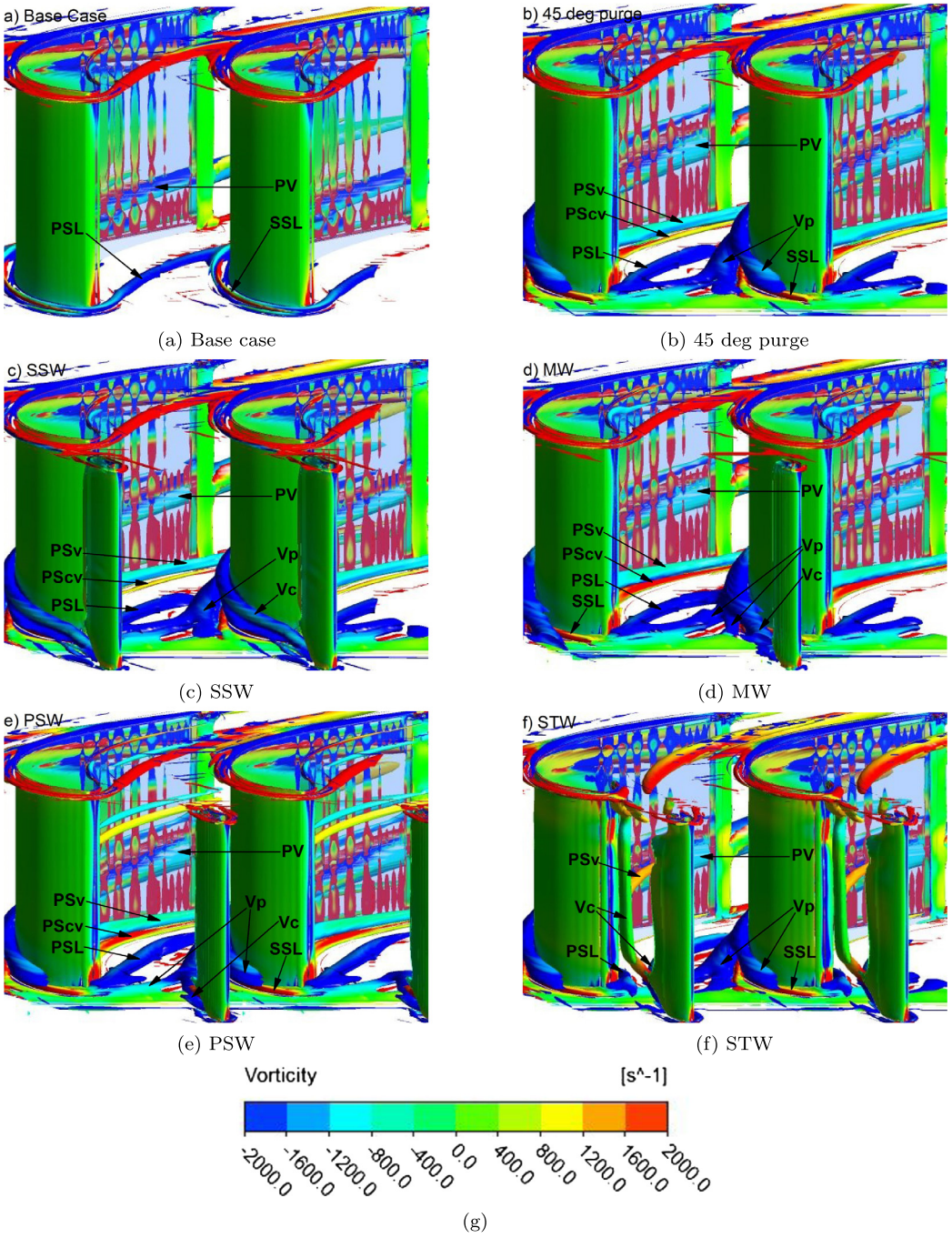

Fig. 7. Leading edge vortex formations for different configurations using Q criterion.

sponsible for the rapidly decreasing value of Cp till X/C_{ax} = 0.3 (Fig. 8a). Further to this location, the static pressure coefficient remains relatively constant until X/C_{ax}=0.5. This trend is common for all the configurations except for STW. It can be seen the static pressure coefficient droops significantly down on blade suction surface ($0.2 < X/C_{ax} < 0.6$) for STW configuration. The cylinder wakes in STW configuration, come in direct contact with the blade leading edge, splits into smaller filaments and move along the pressure and suction surfaces. This is evident from the unsteady analysis (Fig. 11). On the other hand, for other configurations, cylinder wake does not interact directly with the leading edge and hence no splitting up into smaller filaments. Instead, they move towards the suctions surface, under the action of passage cross flow, and slows down the flow near the suction surface. The static pressure coefficients for different cylinder positions near the endwall are shown in Fig. 8b. Static pressure reduction for purge cases remains constant and uniform until X/C_{ax} = 0.15 on suction surface. After that significant variation of Cp value can be observed for base case and purge cases up to blade mid passage. At X/C_{ax} = 0.22, for base case, there is a contour level of C_p = -1.5, as compared with the 45 degree purge case, showing just a small region having a minimum value of C_p = -0.1. This is due to the strong recirculation zones generated by the deceleration of endwall boundary layer by the purge flow. For all configurations with upstream cylinders, varying C_p values are explored in between $0.2 < X/C_{ax} < 0.5$ on the suction surface because of more disturbed secondary flows formed at the merging point of additional vortices (Vp and Vc) with the SSL. As cylinder shifts from suction to pressure side, the

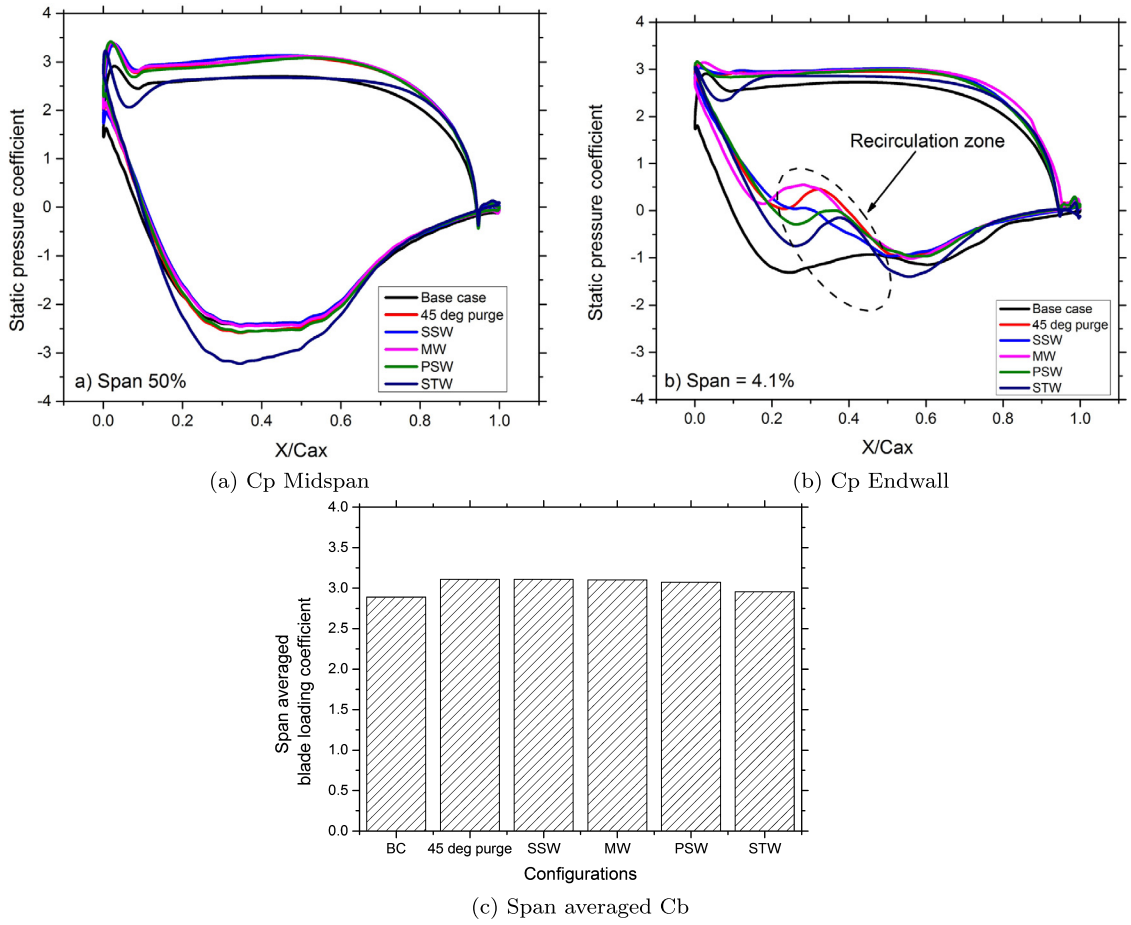

Fig. 8. Static pressure coefficient (Cp) and span averaged blade loading coefficient (Cb) on the blade surface for different configurations.

static pressure distribution over suction surface has decreased and the merging point of Vp and Vc with SSL has shifted downstream. Blade loading coefficient (C_b) of all cases are quantitatively compared in Fig. 8c. C_b is calculated as the difference between the static pressure coefficients (C_p) over blade pressure surface and suction surface. Compared to base case C_b has marginal increase by the introduction of purge flow as well as upstream wakes. Comparing the upstream wake cases, STW configuration is exhibiting the lowest C_b because of the slight but considerable reduction of C_p (Fig. 8a) throughout the pressure surface due to the presence of cylinder vortices. In rest of the upstream wake configurations the cylinder vortices are carried towards the suction surface by the cross flow without disturbing the pressure surface.

The influence of upstream cylinder positions on blade exit yaw angle is explained in Fig. 9. The yaw angle deviation is calculated with respect to exit blade angle and is plotted as contours on a streamwise plane at 120% C_{ax}. Passage vortex (PV) exhibits overturning near the endwall and underturning towards midspan. It is observed that at downstream of the trailing edge, the PV occupies a smaller area, roughly between 15% and 30% of span, for the base case (Fig. 9a). The introduction of purge flow enhances the passage vortex which grows in size both in the spanwise and pitchwise direction. The overturning near the endwall is enhanced by additional purge vortex (Vp) (Fig. 9b). STW configuration exhibits maximum overturning and underturning at about 20% and 40% span respectively. However PSW and STW configurations are capable of pushing secondary flow more close to the endwall. The passage vortex shifts 4% towards the endwall in STW and PSW configurations compared to MW configuration (Fig. 9e & 9f). The stretching of the passage vortex causes an increased underturning in the midpassage region for STW configuration. This is due to the increased interaction of the cylinder vortices with the pressure surface of the blade.

4.3. Analysis through limiting streamlines

The formation of additional flow structures by purge flow and upstream cylinders significantly influence the turbulent kinetic energy (TKE) distribution near to endwall. Fig. 10 shows the turbulent kinetic energy distribution superimposed with limiting streamlines for base case and purge flow with different upstream cylinder locations. Horse shoe vortex and additional upstream vortices generated by purge flow (Vp) are the major causes for high turbulent kinetic energy at fore part of the blade passage. The low momentum purge flow acts as a blockage to the mainstream flow and difference in the velocity magnitudes between purge and mainstream, pushed the saddle point (S1) towards suction side from leading edge (Fig. 10b). Attachment point (A1) of passage cross flow on suction surface is pulled upstream by the additional roll-up vortices generated by purge flow (Fig. 10b). In SSW configuration, purge flow drags the endwall boundary layer partially into the purge slot which stimulates the turbulent mixing near the pressure surface (shown in circle, near pressure surface - Fig. 10c). At the same time fluid ejecting out of the purge slot near suction surface accelerates along the suction surface just downstream of blade leading edge (shown in circle, near suction surface – Fig. 10c). In MW configuration significant TKE reduction is observed at the upstream of the blade passage (shown in circle) due to the interaction of high momentum mainstream with cylinder wakes (Fig. 10d). At the merging point of pressure side leg of horse

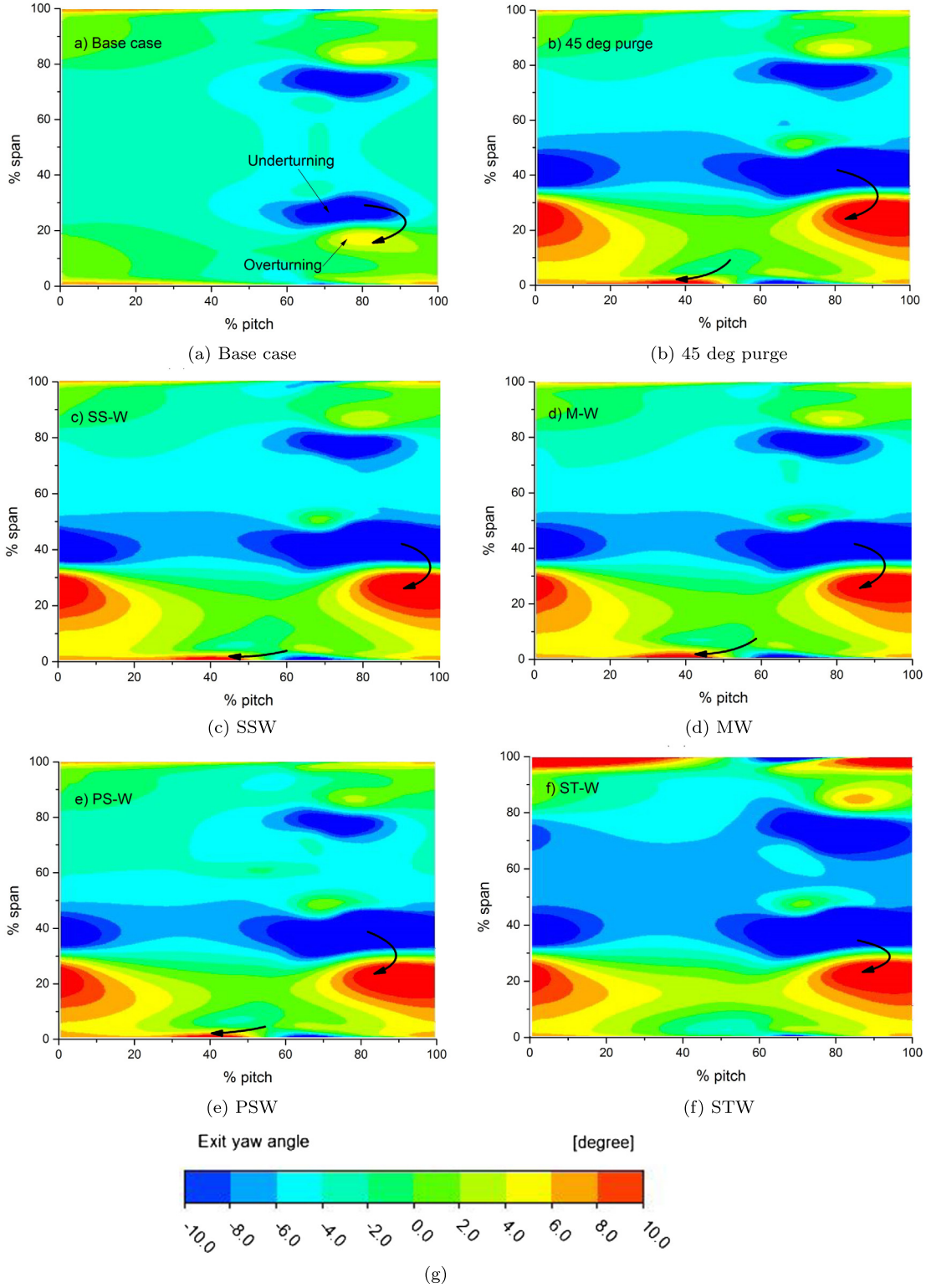

Fig. 9. Exit yaw angle deviation at 120% C_{ax} for different rod configurations.

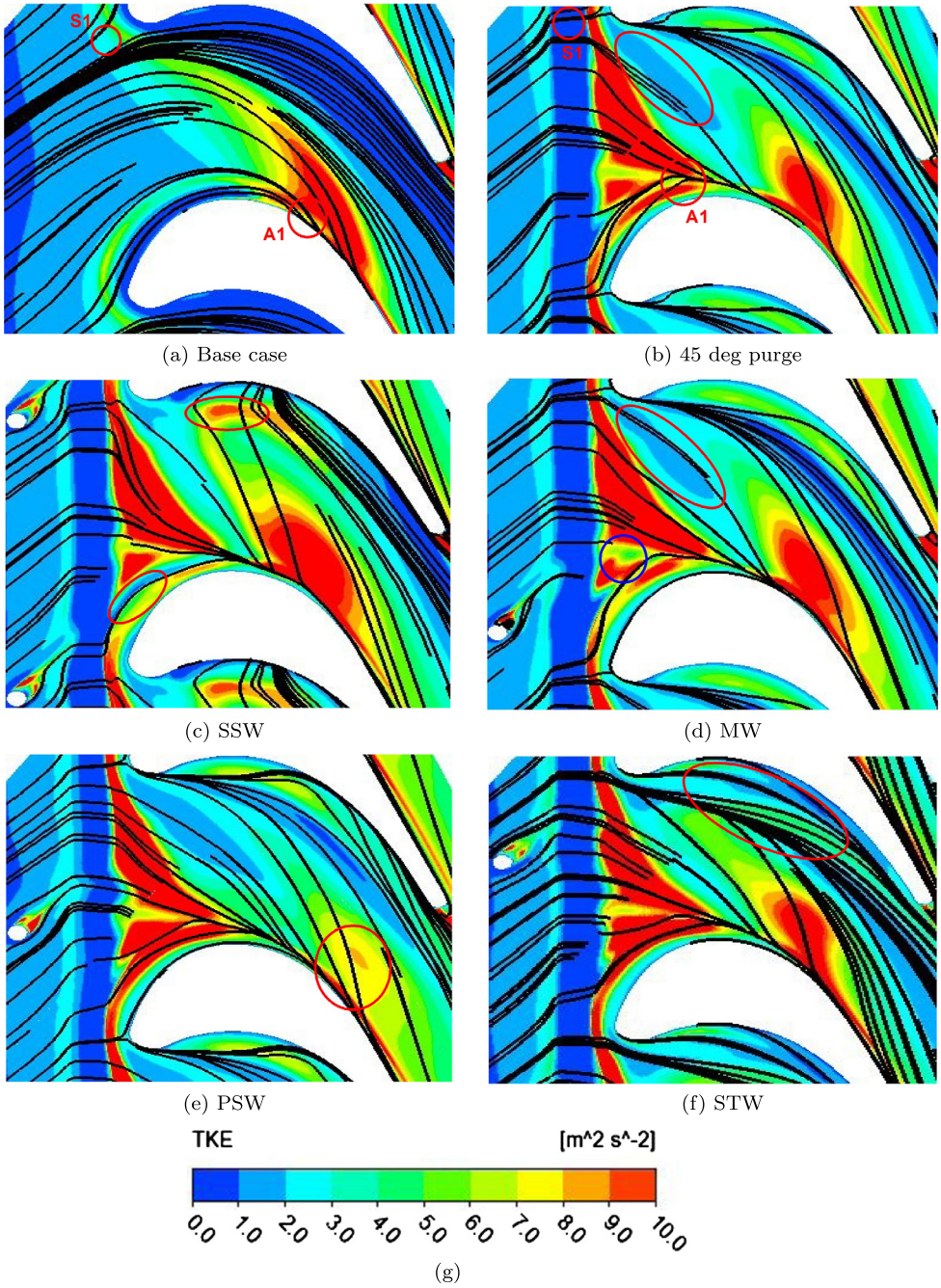

Fig. 10. TKE distribution on endwall for various configurations.

shoe vortex with suction side leg, an enhancement of turbulent kinetic energy is observed. This enhancement is not very prominent in the PSW configuration due to the flow acceleration generated by the cylinder wakes (Fig. 10e). In STW configuration the cylinder wakes (Vc) along the pressure surface, dominates the migration of pressure side leg towards suction side, reduces the TKE distribution along the pressure side-endwall junction which is evident from the limiting streamlines (Fig. 10f). This results in the overall reduction of turbulent kinetic energy distribution over endwall.

4.4. Unsteady analysis of vortex formations at different rod locations

The unsteady analysis gives clear and more accurate information about the evolution and propagation of cylinder vortices and purge vortices and their interaction with the passage vortices. Fig. 11 & 12 shows the unsteady vortex evolution inside the flow passage for two different time instances (τ = 0.0 & 0.5). Q-criterion along with streamwise vorticity has been calculated and plotted for two different configurations viz. STW and MW.

For STW configurations (Fig. 11a) the upstream cylinder vortices are near to the leading edge and hence the back pressure from the leading edge, splits these cylinder vortices (Vc) into different small filaments. These filaments exhibit distinct dynamic behaviors inside the blade passage. The filaments which approach the blade leading edge, again splits into smaller vortices and move along the suction surface and pressure surface. These smaller filaments interacts with the low momentum fluid near the pressure surface boundary layer and generates more intense pressure surface vortices (PSv) that propagates to the downstream. The PSv exist as pairs of vortices having opposite rotational direction. As

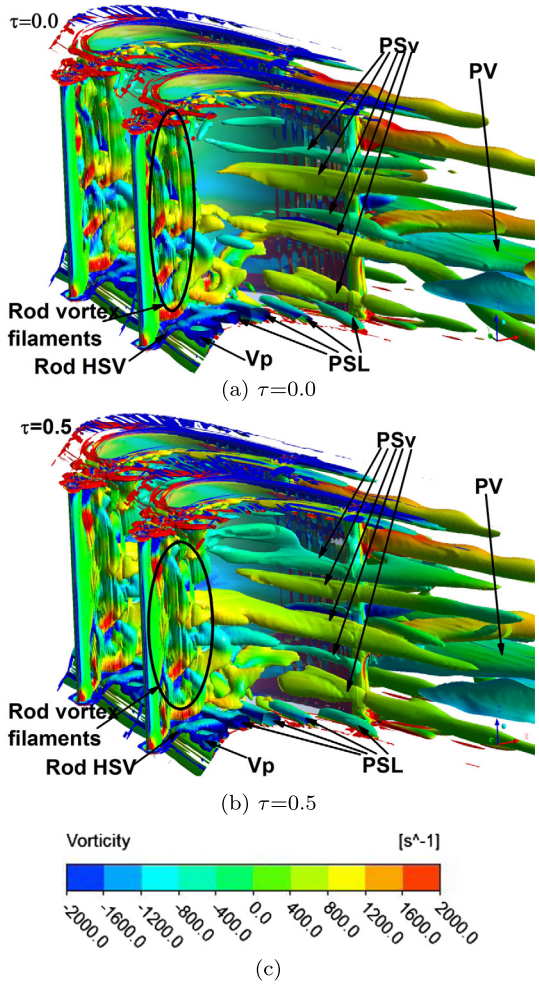

Fig. 11. Q-criterion with streamwise vorticity for STW configuration at τ = 0.0 & 0.5.

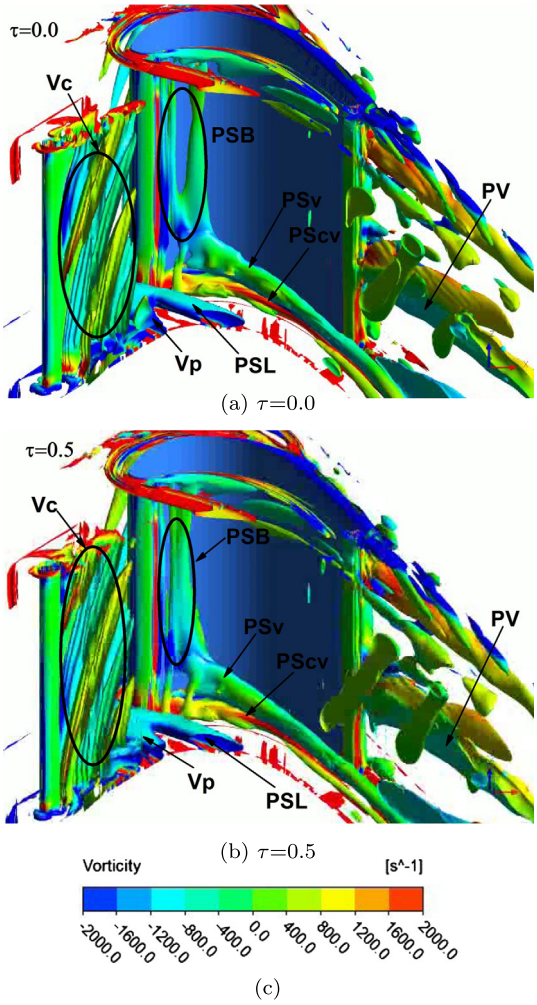

Fig. 12. Q-criterion with streamwise vorticity for MW configuration at τ = 0.0 & 0.5.

this PSv accumulate on the pressure surface, at first, PSL is skewed and later bend near the pressure surface. At τ= 0.5, more pressure surface vortices are observed which are merged together thereby increasing the complexity of passage flow aerodynamics at the exit. Apart from this vortex filaments, at endwall, the cylinder itself generates horse shoe vortex, which interacts with the PSL and leads to the alternate rolling of PSL from leading edge to trailing edge. The pressure surface vortices (PSv) having positive vorticity tends to drag the PSL towards the pressure surface. As a result, tail of the PSL gets skewed and elongated compared to MW configuration. This accelerates the merging of PScv with PSv.

On the contrary, the generations of these pressure surface vortices are limited near to the endwall for MW configuration (Fig. 12). As the upstream wake moves to the mid-passage region their interaction with the purge flow is quite notable in the MW configuration. The kinetic energy of the purge flow is less near the blade leading edge due to the upstream back pressure from the blade leading edge. This gives an added momentum to the purge flow at the mid-passage region and it enters into the mainstream with high kinetic energy. As a result, it creates a blockade to the incoming cylinder vortices near the endwall for MW configuration. This causes the upper portion of the cylinder vortices to propagate faster than the lower portion and create a shearing action for the cylinder vortices along the streamwise direction. In MW configuration, apart from the Karman vortices, the horseshoe vortex generated by the cylinder are broken by the purge flow and both moves towards the suction surface under the influence of the pitchwise pressure gradient.

Secondary vortex interactions along the spanwise direction are explained using streamwise vorticity in Fig. 13. In MW configuration, at midspan region, the Karman vortex street from the upstream cylinder propagates downstream keeping their opposite sense of rotation intact till they dissipate (shown as arrow line). The transport mechanisms exhibited by the alternate vortices are different and there is no direct interaction between them. However, in the region where they interact with the passage vortex, they got stretched and move towards the downstream direction (dashed circle-50% span). On the other hand, closer to the endwall, the Karman vortices are almost engulfed by the horseshoe vortex of the blade leading edge. The positive vortex is swallowed by the SSL and eventually moved towards the suction side of the blade. The negative cylinder vortex combines with the purge vortex, well inside the blade passage slightly away from the suction side. These vortex formations leads to the enhancement of passage vortex having negative vorticity at the blade exit.

The effect of unsteady vortices on the flow field aerodynamics characterized by total pressure loss coefficient at different streamwise planes (10%, 45%, 80% & 120% C_{ax}) are shown in Fig. 14 & 15 for two upstream cylinder positions. Frames at three instances are selected (τ= 0.0, 0.8 and 1.5) for understanding the effect of unsteady vortex structures on the loss coefficient for STW configuration. Each total pressure loss core regions comprises of a pair of pressure surface vortices of opposite sense of rotation as explained in Fig. 11.

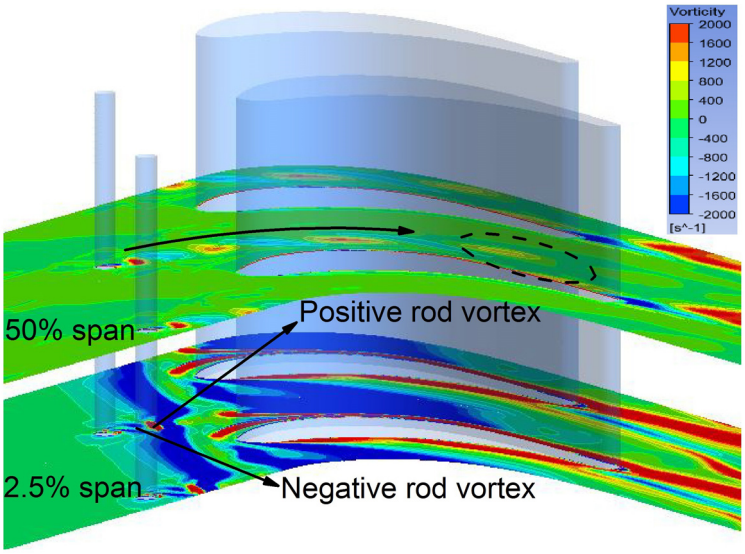

Fig. 13. Spanwise planes vorticity contours for MW configuration at τ=0.0.

At initial time step (τ=0), near to hub endwall, cylinder vortex filament (Fig. 14a, below 40% span, at 10%, 45%, 80% C_{ax}) drags the tail of pressure side leg into it and roll upwards forming endwall pressure surface vortex. Similarly towards midspan, after interacting with the blade leading edge, the cylinder vortices alone will cause the formation of midspan pressure surface vortex (Fig. 14a, 10%, 45%, 80% C_{ax}). These vortices are detached from the pressure surface at different time-steps and enhance the intensity of trailing edge vortices at the downstream. At the exit plane (120% C_{ax}) the pressure surface vortices interacts with endwall loss regions and trailing edge wake regions. The loss core regions corresponding to pressure surface vortices are highlighted at different spanwise locations. The frequency of formation of endwall pressure surface vortices is higher than midspan pressure surface vortices. Endwall PSv separates from the pressure side (80% C_{ax} and 25% span) at τ= 0.8 (Fig. 14b), while midspan PSv will enlarge in size and shift spanwise direction and detach from pressure surface (80% C_{ax} and 70% span) at τ=1.5 (Fig. 14c). At 120% C_{ax}, detached, endwall and midspan PSv from pressure surface merges with trailing edge wall vortex (WV) and trailing edge wake regions respectively (Fig. 14c). This interaction increases the overall loss coefficient inside the blade passage and blade exit region.

The unsteady vortex evolution for MW configuration is obtained from two frames (τ = 0.0 & 0.45) shown in Fig. 15. In MW configurations, τ=0.0, the endwall portion of the cylinder vortices are dragged into the passage vortex by the boundary layer cross flow. As a result rather than trailing edge wake regions, the passage vortex loss core regions are much more intense in this case. The loss core region marked by black circle (Fig. 15a, 10% C_{ax}) shows the presence of cylinder vortex (Vc). It passes the blade passage independently not interfering with the blade surfaces except at endwall. This can be observed from planes located at 80% and 120% C_{ax} (18% and 30% span respectively). At τ=0.45, near to the hub region intervention of cylinder vortex with the passage vortex results in the squeezing of the same in spanwise direction by 3% at 80% C_{ax} and 5% at 120% C_{ax} (Fig. 15b). Also the small loss core region appears strong but confined at the hub represents the pressure surface vortex residuals. Present numerical investigation confirms that rotational direction and lateral position of cylinder vortices place a crucial role in the evolution of secondary flow within the blade passage and blade exit region for a low aspect ratio turbine blade.

5. Conclusions

The interaction of upstream wakes with the purge flow inside a turbine blade cascade has been numerically investigated in the presence of upstream wakes generated from a cylindrical rod. The generation of wake from four pitchwise locations has been analyzed separately and subsequent modifications in the secondary flow has been investigated.

It is observed that shifting of upstream cylinder from SSW to STW configuration has a huge influence on the downstream exit flow angle deviation which can definitely alters the flow characteristics of succeeding blade rows. The merging point of suction side leg and pressure side leg of horse shoe vortex shift towards the aft part of blade passage under the influence of cylinder vortices. The unsteady analysis reveals the formation of filament type vortical structures and its propagation inside the blade passage. In STW configuration, these vortical structures splits across blade leading edge into two legs having different rotational directions. The formation of pressure surface vortices (PSv) and its interaction with the blade trailing edge wake regions amplify blade exit unsteadiness and cause additional loss generation compared to MW configuration. Apart from these vortex filaments, at endwall, the cylinder itself generates horse shoe vortex, which interacts with the PSL and leads to the alternate rolling of PSL from leading edge to trailing edge. In MW configuration, the horseshoe vortex generated by the cylinder is broken by the purge flow. The obstruction created by the purge flow causes the upper portion of cylinder vortices to bend forward, creating a shearing action along the spanwise direction. The unsteady analysis reveals that, in STW configuration, the frequency of formation of pressure surface vortices at midspan is smaller than near the endwall. Present numerical investigation confirms that, interaction of upstream wakes with purge flow plays a major role in the evolution of secondary flow within the blade passage and blade exit region for a low aspect ratio turbine blade. The results presented in this paper depend on specific turbine geometry and stationary upstream wakes. So care should be taken while generalizing the results.

Declaration of competing interest

The authors declare that they have no known competing financial interests or personal relationships that could have appeared to influence the work reported in this paper.

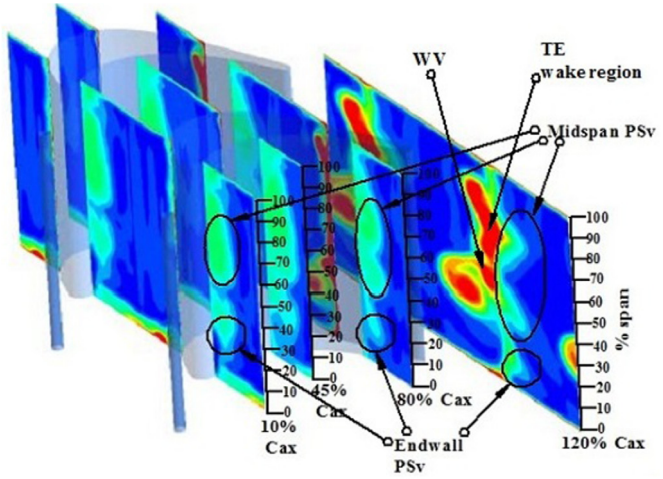

(a) τ=0.0

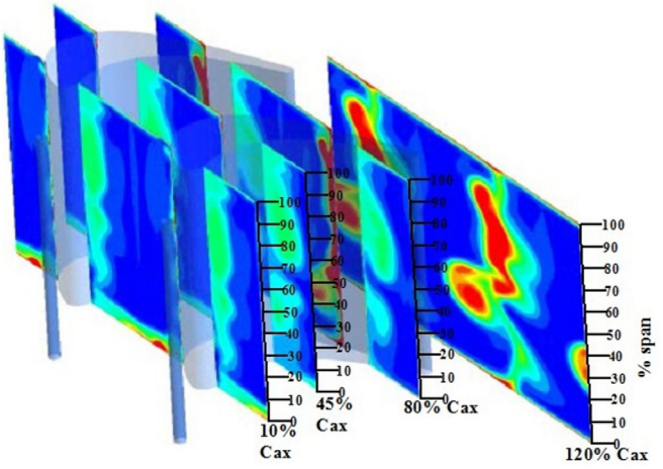

(b) τ=0.8

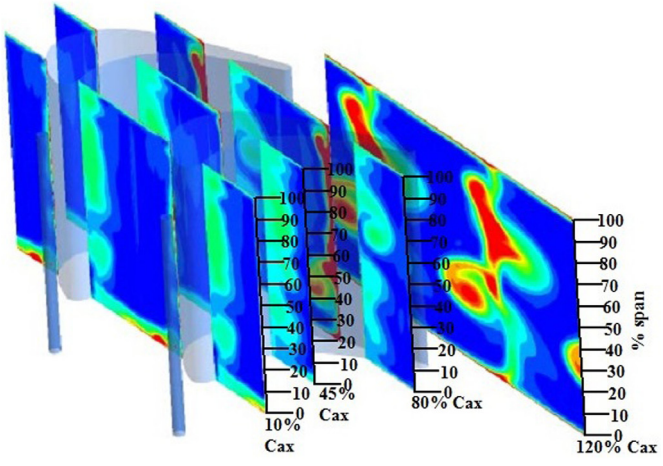

(c) τ=1.5

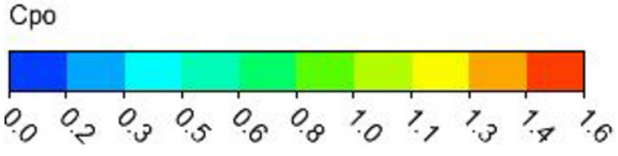

(d)

Fig. 14. Total pressure loss coefficient at different streamwise planes for STW configuration.

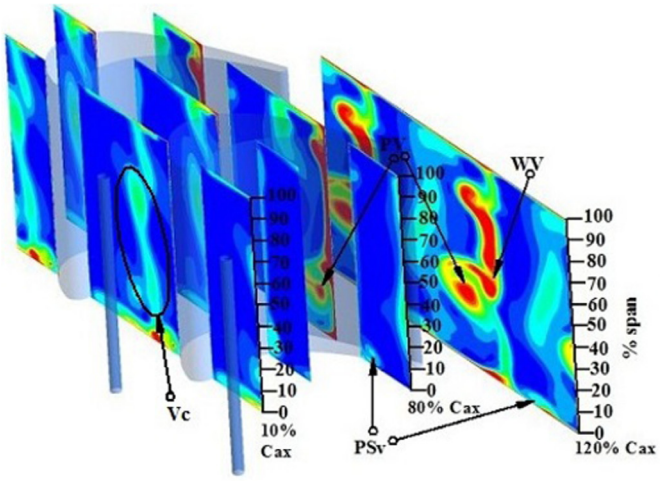

(a) τ=0.0

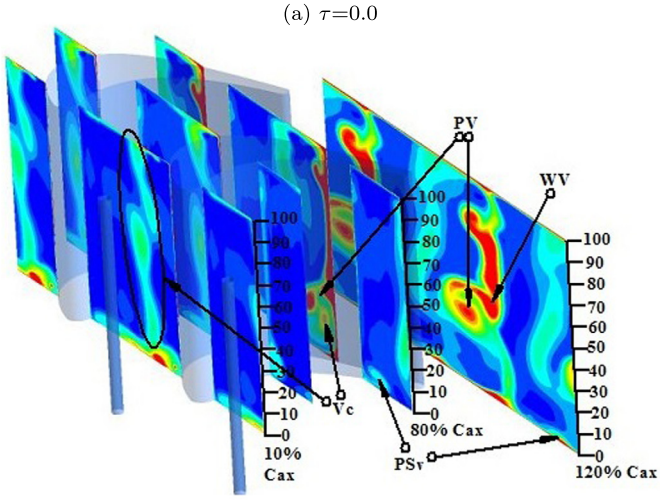

(b) τ=0.45

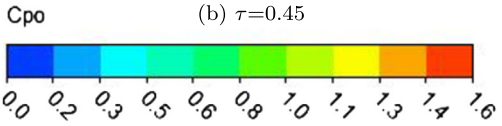

(c)

Fig. 15. Total pressure loss coefficient at different streamwise planes for MW configuration.

Acknowledgements

The authors gratefully acknowledge the technical support by National Institute of Technology Karnataka (NITK).

References

[1] Zuo-Jun Wei, Wei-Yang Qiao, Jian Liu, Wen-Hua Duan, Reduction of endwall secondary flow losses with leading-edge fillet in a highly loaded low-pressure turbine, Proc. Inst. Mech. Eng. A, J. Power Energy 230 (2) (2016) 184–195.

[2] G.A. Zess, Karen Ann Thole, Computational design and experimental evaluation of using a leading edge fillet on a gas turbine vane, J. Turbomach. 124 (2) (2002) 167–175.

[3] K. Ananthakrishnan, M. Govardhan, Influence of fillet shapes on secondary flow field in a transonic axial flow turbine stage, Aerosp. Sci. Technol. 82 (2018) 425–437.

[4] Krishna Nandan Kumar, M. Govardhan, Secondary flow loss reduction in a turbine cascade with a linearly varied height streamwise endwall fence, Int. J. Rotating Mach. 2011 (2011).

[5] Rongfei Yang, Dongdong Zhong, Ning Ge, Numerical investigation on flow control effects of dynamic hump for turbine cascade at different Reynolds number and hump oscillating frequency, Aerosp. Sci. Technol. (2019).

[6] Özhan H. Turgut, Cengiz Camcı, A nonaxisymmetric endwall design approach and its computational assessment in the NGV of an HP turbine stage, Aerosp. Sci. Technol. 47 (2015) 456–466.
[7] Zhendong Guo, Hongyan Bu, Liming Song, Jun Li, Zhenping Feng, Experimental test of a 3D parameterized vane cascade with non-axisymmetric endwall, Aerosp. Sci. Technol. 85 (2019) 429–442.
[8] Yuxi Luo, Fengbo Wen, Shuai Wang, Shibo Zhang, Songtao Wang, Zhongqi Wang, Numerical investigation on the biomimetic trailing edge of a high-subsonic turbine blade, Aerosp. Sci. Technol. 89 (2019) 230–241.
[9] S. Friedrichs, H.P. Hodson, W.N. Dawes, Distribution of film-cooling effectiveness on a turbine endwall measured using the ammonia and diazo technique, in: ASME 1995 International Gas Turbine and Aeroengine Congress and Exposition, American Society of Mechanical Engineers Digital Collection, 1995.
[10] S. Friedrichs, H.P. Hodson, W.N. Dawes, The design of an improved endwall film-cooling configuration, J. Turbomach. 121 (4) (1999) 772–780.
[11] S. Friedrichs, H.P. Hodson, W.N. Dawes, Aerodynamic aspects of endwall film-cooling, J. Turbomach. 119 (4) (1997) 786–793.
[12] Giovanna Barigozzi, Giuseppe Benzoni, Giuseppe Franchini, Antonio Perdichizzi, Fan-shaped hole effects on the aero-thermal performance of a film-cooled endwall, J. Turbomach. 128 (1) (2006) 43–52.
[13] Giovanna Barigozzi, Giuseppe Franchini, A. Perdichizzi, Massimiliano Maritano, Roberto Abram, Influence of purge flow injection angle on the aerothermal performance of a rotor blade cascade, J. Turbomach. 136 (4) (2014) 041012.
[14] Giovanna Barigozzi, Giuseppe Franchini, Antonio Perdichizzi, Silvia Ravelli, Effects of trenched holes on film cooling of a contoured endwall nozzle vane, J. Turbomach. 134 (4) (2012) 041009.
[15] Giovanna Barigozzi, Antonio Perdichizzi, Silvia Ravelli, Pressure side and cut-back trailing edge film cooling in a linear nozzle vane cascade at different Mach numbers, J. Turbomach. 134 (5) (2012) 051037.
[16] Jie Gao, Ming Wei, Weiliang Fu, Qun Zheng, Guoqiang Yue, Experimental and numerical investigations of trailing edge injection in a transonic turbine cascade, Aerosp. Sci. Technol. (2019).
[17] R.P. Roy, K.D. Squires, M. Gerendas, S. Song, W.J. Howe, A. Ansari, Flow and heat transfer at the hub endwall of inlet vane passages—experiments and simulations, in: ASME Turbo Expo 2000: Power for Land, Sea, and Air, American Society of Mechanical Engineers Digital Collection, 2000.
[18] Vishal Venkatesh, J. Sriraam, K. Subhash, Ratna Kishore Velamati, A.R. Srikrishnan, Balajee Ramakrishnananda, Suresh Batchu, Studies on effusion cooling: impact of geometric parameters on cooling effectiveness and coolant consumption, Aerosp. Sci. Technol. 77 (2018) 58–66.
[19] Chunhua Wang, Jingzhou Zhang, Junhui Zhou, Optimization of a fan-shaped hole to improve film cooling performance by RBF neural network and genetic algorithm, Aerosp. Sci. Technol. 58 (2016) 18–25.
[20] Steven W. Burd, Terrence W. Simon, Effects of slot bleed injection over a contoured endwall on nozzle guide vane cooling performance: part I—flow field measurements, in: ASME Turbo Expo 2000: Power for Land, Sea, and Air, American Society of Mechanical Engineers Digital Collection, 2000.
[21] Rohit A. Oke, Terrence W. Simon, Steven W. Burd, Rickard Vahlberg, Measurements in a turbine cascade over a contoured endwall: discrete hole injection of bleed flow, in: ASME Turbo Expo 2000: Power for Land, Sea, and Air, American Society of Mechanical Engineers Digital Collection, 2000.
[22] Friedrich Kost, Martin Nicklas, Film-cooled turbine endwall in a transonic flow field: part I—aerodynamic measurements, J. Turbomach. 123 (4) (2001) 709–719.
[23] Kevin Liu, Shang-Feng Yang, Je-Chin Han, Influence of coolant density on turbine platform film-cooling with stator–rotor purge flow and compound-angle holes, J. Therm. Sci. Eng. Appl. 6 (4) (2014) 041007.
[24] Martin Nicklas, Film-cooled turbine endwall in a transonic flow field: part II—heat transfer and film-cooling effectiveness, J. Turbomach. 123 (4) (2001) 720–729.
[25] A. Suryanarayanan, S.P. Mhetras, M.T. Schobeiri, J.C. Han, Film-cooling effectiveness on a rotating blade platform, J. Turbomach. 131 (1) (2009) 011014.
[26] Gaowen Liu, Songling Liu, Huiren Zhu, B.L. Lapworth, A.E. Forest, Endwall heat transfer and film cooling measurements in a turbine cascade with injection upstream of leading edge, Heat Transf. Asian Res. 33 (3) (2004) 141–152, Co-sponsored by the Society of Chemical Engineers of Japan and the Heat Transfer Division of ASME.
[27] M. Papa, Vinod Srinivasan, Richard J. Goldstein, Film cooling effect of rotor-stator purge flow on endwall heat/mass transfer, J. Turbomach. 134 (4) (2012) 041014.
[28] Andrew F. Chen, Chao-Cheng Shiau, Je-Chin Han, Turbine blade platform film cooling with simulated swirl purge flow and slashface leakage conditions, J. Turbomach. 139 (3) (2017) 031012.
[29] Nafiz H.K. Chowdhury, Chao-Cheng Shiau, Je-Chin Han, Luzeng Zhang, Hee-Koo Moon, Turbine vane endwall film cooling with slashface leakage and discrete hole configuration, J. Turbomach. 139 (6) (2017) 061003.
[30] Jiahuan Cui, Paul Tucker, Numerical study of purge and secondary flows in a low-pressure turbine, J. Turbomach. 139 (2) (2017) 021007.
[31] J-C. Han, L. Zhang, S. Ou, Influence of unsteady wake on heat transfer coefficient from a gas turbine blade, J. Heat Transf. 115 (4) (1993) 904–911.
[32] Shichuan Ou, J-C. Han, Anant B. Mehendale, C. Pang Lee, Unsteady wake over a linear turbine blade cascade with air and CO2 film injection: part I—effect on heat transfer coefficients, J. Turbomach. 116 (4) (1994) 721–729.
[33] Anant B. Mehendale, J-C. Han, Shichuan Ou, C. Pang Lee, Unsteady wake over a linear turbine blade cascade with air and CO2 film injection: part II—effect on film effectiveness and heat transfer distributions, J. Turbomach. 116 (4) (1994) 730–737.
[34] L. Zhang, J-C. Han, Influence of mainstream turbulence on heat transfer coefficients from a gas turbine blade, J. Heat Transf. 116 (4) (1994) 896–903.
[35] L. Zhang, J-C. Han, Combined effect of free-stream turbulence and unsteady wake on heat transfer coefficients from a gas turbine blade, J. Heat Transf. 117 (2) (1995) 296–302.
[36] Yifei Li, Xinrong Su, Xin Yuan, The effect of mismatching between combustor and HP vanes on the aerodynamics and heat load in a 1-1/2 stages turbine, Aerosp. Sci. Technol. 86 (2019) 78–92.
[37] Kai Zhou, Chao Zhou, Unsteady effects of vortex interaction on tip leakage vortex breakdown and its loss mechanism, Aerosp. Sci. Technol. 82 (2018) 363–371.
[38] Stefan Zerobin, Sabine Bauinger, Andreas Marn, Andreas Peters, Franz Heitmeir, Emil Göttlich, The unsteady flow field of a purged high pressure turbine based on mode detection, in: ASME Turbo Expo 2017: Turbomachinery Technical Conference and Exposition, American Society of Mechanical Engineers Digital Collection, 2017.
[39] Stefan Zerobin, Andreas Peters, Sabine Bauinger, Ashwini Bhadravati Ramesh, Michael Steiner, Franz Heitmeir, Emil Göttlich, Aerodynamic performance of turbine center frames with purge flows—part I: the influence of turbine purge flow rates, J. Turbomach. 140 (6) (2018).
[40] Stefan Zerobin, Christian Aldrian, Andreas Peters, Franz Heitmeir, Emil Göttlich, Aerodynamic performance of turbine center frames with purge flows—part II: the influence of individual hub and tip purge flows, J. Turbomach. 140 (6) (2018) 061010.
[41] Florian Hammer, Neil Sandham, Richard Sandberg, The influence of different wake profiles on losses in a low pressure turbine cascade, Internat. J. Turbomach., Propuls. Power 3 (2) (2018) 10.
[42] Seok Min Choi, Jun Su Park, Heeyoon Chung, Sehjin Park, Hyung Hee Cho, Upstream wake effect on flow and heat transfer characteristics at an endwall of first-stage blade of a gas turbine, Exp. Therm. Fluid Sci. 86 (2017) 23–36.
[43] Santosh Abraham, Kapil Panchal, Srinath V. Ekkad, Wing Ng, Andrew S. Lohaus, Anthony Malandra, Effect of endwall contouring on a transonic turbine blade passage: part 1—aerodynamic performance, in: ASME Turbo Expo 2012: Turbine Technical Conference and Exposition, American Society of Mechanical Engineers Digital Collection, 2012, pp. 1089–1098.
[44] Kapil V. Panchal, Santosh Abraham, Srinath V. Ekkad, Wing Ng, Andrew S. Lohaus, Michael E. Crawford, Effect of endwall contouring on a transonic turbine blade passage: part 2—heat transfer performance, in: ASME Turbo Expo 2012: Turbine Technical Conference and Exposition, American Society of Mechanical Engineers Digital Collection, 2012, pp. 151–161.
[45] Arnab Roy, Sakshi Jain, Srinath V. Ekkad, Wing F. Ng, Andrew S. Lohaus, Michael E. Crawford, Heat transfer performance of a transonic turbine blade passage in presence of leakage flow through upstream slot and mateface gap with endwall contouring, in: ASME Turbo Expo 2014: Turbine Technical Conference and Exposition, American Society of Mechanical Engineers Digital Collection, 2014.
[46] Lesley M. Wright, Sarah A. Blake, Dong-Ho Rhee, Je-Chin Han, Effect of upstream wake with vortex on turbine blade platform film cooling with simulated stator-rotor purge flow, J. Turbomach. 131 (2) (2009) 021017.
[47] Dwain I. Dunn, Glen C. Snedden, T.W. Von Backström, Turbulence model comparisons for a low pressure 1.5 stage test turbine, 2009.
[48] O. Turgut, Cengiz Camcı, A nonaxisymmetric endwall design methodology for turbine nozzle guide vanes and its computational fluid dynamics evaluation, in: ASME 2011 International Mechanical Engineering Congress and Exposition, American Society of Mechanical Engineers Digital Collection, 2012, pp. 37–49.
[49] K.N. Kiran, S. Anish, An investigation on the effect of pitchwise endwall design in a turbine cascade at different incidence angles, Aerosp. Sci. Technol. 71 (2017) 382–391.
[50] M.T. Schobeiri, K. Lu, M. Rezasoltani, Effect of non-axisymmetric contouring on performance and film cooling of a rotating turbine endwall subjected to the secondary air purge: a combined numerical and experimental study, Proc. Inst. Mech. Eng. A, J. Power Energy 229 (8) (2015) 813–831.
[51] Rohit A. Oke, Terrence W. Simon, Film cooling experiments with flow introduced upstream of a first stage nozzle guide vane through slots of various geometries, in: ASME Turbo Expo 2002: Power for Land, Sea, and Air, American Society of Mechanical Engineers Digital Collection, 2002, pp. 33–40.
[52] C.M. Schneider, D. Schrack, M. Kuerner, M.G. Rose, S. Staudacher, Y. Guendogdu, U. Freygang, On the unsteady formation of secondary flow inside a rotating turbine blade passage, J. Turbomach. 136 (6) (2014) 061004.
[53] Remo Marini, Sami Girgis, The effect of blade leading edge platform shape on upstream disk cavity to mainstream flow interaction of a high-pressure turbine stage, in: ASME Turbo Expo 2007: Power for Land, Sea, and Air, American Society of Mechanical Engineers Digital Collection, 2007, pp. 587–596.

[54] W. Ghopa Wan Aizon, Ken-ichi Funazaki, Takemitsu Miura, Purge flow effect on aerodynamics performance in high-pressure turbine cascade, J. Mech. Sci. Technol. 27 (6) (2013) 1611–1617.
[55] A. Asghar, W.D.E. Allan, M. LaViolette, R. Woodason, Influence of a novel 3D leading edge geometry on the aerodynamic performance of low pressure turbine blade cascade vanes, in: ASME Turbo Expo 2014: Turbine Technical Conference and Exposition, American Society of Mechanical Engineers Digital Collection, 2014.